Supplementary Materials for

Structural basis of transcription activation

Yu Feng, Yu Zhang, and Richard H. Ebright

correspondence to: ebright@waksman.rutgers.edu

This PDF file includes:

Materials and Methods

T. thermophilus transcription activator protein TTHB099

E. coli strain BL21(DE3) (Invitrogen, Inc.) was transformed with plasmid pET28a-TTHB099 [constructed by replacement of the NdeI-BamHI segment of plasmid pET28a (EMD Millipore, Inc.) by the NdeI-BamHI DNA segment of a gene-synthesis-derived DNA fragment carrying CAT, followed by codons 1-195 of the *T. thermophilus* TTHB099 gene (5), followed by TGAGGATCC (GenScript, Inc.)], encoding N-hexahistidine-tagged *T. thermophilus* TAP under control of the bacteriophage T7 gene 10 promoter, or with a pET28a-TTHB099 derivative constructed by use of site-directed mutagenesis (QuikChange Site-Directed Mutagenesis Kit; Agilent, Inc.). Single colonies of the resulting transformants were used to inoculate 50 ml LB broth containing 50 μg/ml kanamycin, and cultures were incubated 16 h at 37°C with shaking. Aliquots (10 ml) were used to inoculate 1 L LB broth containing 50 μg/ml kanamycin, cultures were incubated at 37°C with shaking until OD_{600} = 0.6, cultures were induced by addition of IPTG to 1 mM, and cultures were incubated an additional 3 h at 37°C. Cells were harvested by centrifugation (5,000 x g; 15 min at 4°C), re-suspended in 20 ml buffer A (20 mM Tris-HCl, pH 7.9, 0.2 M NaCl) and lysed using an EmulsiFlex-C5 cell disrupter (Avestin, Inc.). Following incubation for 13 min at 70°C, the lysate was centrifuged (20,000 x g; 30 min at 4°C), and the supernatant was loaded onto a 5 ml column of Ni-NTA-agarose (Qiagen, Inc.) equilibrated in buffer A. The column was washed with 50 ml buffer A containing 40 mM imidazole and eluted with 25 ml buffer A containing 0.5 M imidazole. The eluate was dialyzed three times against 1 L 20 mM Tris-HCl (pH7.7), 0.5 M NaCl, and 5% glycerol, and was stored at -80°C. Yields were ~10 mg/L, and purities were >95%.

Fluorescein-labelled TAP ([fluorescein-Cys133]TAP) was prepared by incubation of 50 μM single-Cys TAP derivative [Cys133]TAP and 1 mM 5-iodoacetamidofluorescein (ThermoFisher, Inc.) in 3 ml 10 mM Na_2HPO_4 (pH 7.4), 2 mM KH_2PO_4, 140 mM NaCl, and 3 mM KCl for 2 h at 25°C, purified by gel-filtration chromatography on a PD-10 column (GE Healthcare, Inc.) in the same buffer, and stored at -80°C.

T. thermophilus αCTD

E. coli strain BL21(DE3) (Invitrogen, Inc.) was transformed with plasmid pET28a-Tt-H6-αCTDCys, encoding N-hexahistidine-tagged *T. thermophilus* RNAP α subunit residues 253-310 followed by a single cysteine residue under control of the bacteriophage T7 gene 10 promoter [constructed by replacement of the NdeI-EcoRI segment of plasmid pET28a (EMD Millipore, Inc.) by the NdeI-EcoRI DNA segment of a gene-synthesis-derived DNA fragment carrying CATATG, followed by codons 253-310 of the *T. thermophilus* TTHB099 gene, followed by TGTTAGGAATTC (GenScript, Inc.)]. A single colony of the resulting transformant was used to inoculate 50 ml LB broth containing 50 μg/ml kanamycin, and the culture was incubated 16 h at 37°C with shaking. A 10 ml aliquot was used to inoculate 1 L LB broth containing 50 μg/ml kanamycin, the culture was incubated at 37°C with shaking until OD_{600} = 0.6, the culture was induced by addition of IPTG to 1 mM, and the culture was incubated an additional 3 h at 37°C. Cells were harvested by centrifugation (5,000 x g; 15 min at 4°C), re-suspended in 20 ml buffer B (50 mM Tris-HCl, pH 7.9, 0.2 M NaCl, 10 mM β-mercaptoethanol) and lysed using an EmulsiFlex-C5 cell disrupter (Avestin, Inc.). The lysate was incubated 20 min at 60°C and centrifuged (20,000 x g; 30 min at 4°C), and the supernatant was loaded onto a 5 ml column of Ni-NTA-agarose (Qiagen, Inc.) equilibrated with buffer B. The column was washed with 50 ml buffer B containing 20 mM imidazole and eluted with 25 ml buffer B containing 0.1 M imidazole. The eluate was dialyzed three times against 1 L 10 mM Na_2HPO_4 (pH 7.4), 2 mM KH_2PO_4, 140 mM NaCl, and 3 mM KCl, and was stored at -80°C. Yields were ~10 mg/L, and purities were >95%.

Fluorescein-labelled αCTD ([fluorescein-Cys311]αCTD) was prepared by incubation of 50 μM [Cys311]αCTD and 1 mM 5-iodoacetamidofluorescein (ThermoFisher, Inc.) in 3 ml 10 mM Na_2HPO_4 (pH 7.4), 2 mM KH_2PO_4, 140 mM NaCl, and 3 mM KCl for 2 h at 25°C, purified by gel-filtration chromatography on a PD-10 column (GE Healthcare, Inc.) in the same buffer, and stored at -80°C.

T. thermophilus σ^A

T. thermophilus σ^A and σ^A derivatives were prepared as in *7*, using plasmid pET28a-Tt-σ^A (*7*; gift of K. Kuznedelov and K. Severinov) and pET28a-Tt-σ^A derivatives constructed using site-directed mutagenesis (QuikChange Site-Directed Mutagenesis Kit; Agilent, Inc.). Yields were ~20 mg/L, and purities were >95%.

T. thermophilus RNAP core enzyme

For structural studies, *T. thermophilus* RNAP core enzyme was prepared as in *7*.

For biochemical studies, *T. thermophilus* RNAP core enzyme and RNAP core enzyme derivatives were prepared as follows: *E. coli* strain BL21 Star (DE3) (Invitrogen, Inc.) was transformed with plasmid pET28a-TthABCZ (gift of K. Kuznedelov and K. Severinov)--encoding *T. thermophilus* RNAP α subunit, β subunit, N-hexahistidine-tagged β' subunit, and ω subunit under control of the bacteriophage T7 gene 10 promoter--or a pET28a-TthABCZ derivative constructed by use of site-directed mutagenesis (QuikChange Site-Directed Mutagenesis Kit; Agilent, Inc.). Single colonies of the resulting transformants were used to inoculate 50 ml LB broth containing 50 μg/ml kanamycin, and cultures were incubated 5.5 h at 30°C with shaking. Aliquots (10 ml) were used to inoculate 1 L LB broth containing 50 μg/ml kanamycin, and cultures were incubated an additional 16 h at 30°C. Cells were harvested by centrifugation (5,000 x g; 15 min at 4°C), re-suspended in 30 ml buffer C (25 mM Tris-HCl, pH 7.9, 0.5 M NaCl, and 10 mM β-mercaptoethanol) and lysed using an EmulsiFlex-C5 cell disrupter (Avestin, Inc.). The lysate was incubated 20 min at 75°C and centrifuged (20,000 x g; 30 min at 4°C). The supernatant was mixed with 0.5% polyethylenimine, stirred 10 min at 4°C, and centrifuged (20,000 x g; 15 min at 4°C). RNAP in the supernatant was precipitated by addition of 29.1 g ammonium sulfate. The pellet was dissolved in 15 ml buffer C and loaded onto a 5 ml column of Ni-NTA-agarose (Qiagen, Inc.) equilibrated with buffer C. The column was washed with 50 ml buffer C containing 10 mM imidazole and eluted with 25 ml buffer C containing 150 mM imidazole. The sample was further purified by anion-exchange chromatography on a 16/10 Mono Q column (GE Healthcare, Inc.; 160 ml linear gradient of 0.25-1 M NaCl in 10 mM Tris-HCl, pH 7.7, 1 mM EDTA, 1 mM dithiothreitol, and 5% glycerol; flow rate = 1 ml/min). Fractions containing RNAP were pooled and stored at -80°C. Yields were ~5 mg/L, and purities were >95%.

T. thermophilus RNAP holoenzyme

For structural studies, *T. thermophilus* RNAP holoenzyme was prepared as in *7*.

For biochemical studies, *T. thermophilus* RNAP holoenzyme and RNAP holoenzyme derivatives were prepared as follows: *T. thermophilus* RNAP core enzyme or RNAP core enzyme derivative (3 μM) and *T. thermophilus* σ^A or σ^A derivative (12 μM) were equilibrated in 1.5 ml 10 mM Tris-HCl (pH 7.7), 350 mM NaCl, 1 mM EDTA, 1 mM dithiothreitol, and 5% glycerol for 2 h at 4°C. The reaction mixture was applied to a HiLoad 16/60 Superdex S200 column (GE Healthcare, Inc.) equilibrated in 20 mM Tris-HCl (pH 7.7), 0.1 M NaCl, and 1% glycerol, and the column was eluted with 120 ml of the same buffer. Fractions containing RNAP holoenzyme were pooled, concentrated to ~3 mg/ml using Amicon Ultra-15 centrifugal ultrafilters (30 kDa MWCO; Millipore, Inc.), and stored at -80°C.

E. coli CAP

E. coli CAP and CAP derivatives were prepared as in (*21*), but using plasmid pAKCRP (*22*) and pAKCRP derivatives constructed using site-directed mutagenesis (QuikChange Site-Directed Mutagenesis Kit; Agilent, Inc.). Yields were ~10 mg/L, and purities were >95%.

E. coli σ^{70}

E. coli σ^{70} and σ^{70} derivatives were prepared as in (*23*), but using plasmid pGEMD (*24*) and pGEMD derivatives constructed using site-directed mutagenesis (QuikChange Site-Directed Mutagenesis Kit; Agilent, Inc.). Yields were ~10-60 mg/L, and purities were >95%.

E. coli RNAP core enzyme

E. coli RNAP core was prepared from *E. coli* strain BL21(DE3) (Invitrogen, Inc.) transformed with plasmids pEcABC-H6 (*4*) and pCDF-ω (*25*), using culture and induction procedures essentially as in *4* and using protein purification procedures essentially as in *23*. Yields were ~2.5 mg/L, and purities were >95%.

E. coli RNAP holoenzyme

For experiments assessing effects of substitutions of residues of RNAP β subunit, *E. coli* RNAP holoenzyme and substituted RNAP holoenzyme derivatives were prepared from *E. coli* strain XE54 (*26*) transformed with plasmid pRL706 (*27*) and pRL706 derivatives constructed using site-directed mutagenesis (QuikChange Site-Directed Mutagenesis Kit; Agilent, Inc.), using procedures as in *28*.

For experiments assessing effects of substitutions of residues of σ^{70}, *E. coli* RNAP holoenzyme and substituted RNAP holoenzyme derivatives were prepared from *E. coli* RNAP core and σ^{70} or substituted σ^{70} derivatives as in *7*).

For hydroxyl-radical DNA footprinting, *E. coli* RNAP holoenzyme and an RNAP holoenzyme lacking αCTD [α(1-235)-RNAP] were prepared by reconstitution from recombinant subunits as in *29*.

Oligonucleotides

Oligodeoxyribonucleotides and oligoribonucleotides (IDT, Inc.) were dissolved in nuclease-free water (Ambion, Inc.) to desired concentrations and stored at -80°C. Ribodinucleotides ApA and ApU (RiboMed, Inc.) were dissolved in nuclease-free water (Ambion, Inc.) to 10 mM and stored at -80°C.

Nucleic-acid scaffolds

The nucleic-acid scaffold for crystallization was prepared as follows: Nontemplate-strand oligodeoxyribonucleotide (0.28 mM), template-strand oligodeoxyribonucleotide (0.31 mM), and oligoribonucleotide (0.56 mM) in 36 µl 5 mM Tris-HCl, pH 7.7, 0.2 M NaCl, and 10 mM $MgCl_2$ were heated 5 min at 95°C, cooled to 25°C in 2°C steps with 1 min per step using a thermal cycler (Applied Biosystems, Inc.) and stored at -80°C.

Promoter DNA fragments

Promoter DNA fragments for transcription assays were prepared by PCR amplification of a synthetic oligodeoxyribonucleotide corresponding to the nontemplate strand of positions -80 to +20 of the *T. thermophilus crtB* promoter (*30*) or the nontemplate strand of positions -77 to +20 of the CC(-41.5) promoter (*31*), were purified using the QIAquick PCR Purification Kit (Qiagen, Inc.), and were stored at -80°C.

Promoter DNA fragments for electrophoretic-mobility-shift assays were prepared as described above for nucleic-acid scaffolds, but using 10 µM Cy5-5'-end-labeled nontemplate-strand and 10 µM template-strand oligodeoxyribonucleotide corresponding to positions -65 to +20 of the λP_R-P_{RMup} promoter (*32*).Promoter DNA fragments for hydroxyl-radical DNA footprinting were prepared as described above for nucleic-acid scaffolds, but using 0.2 µM ^{32}P-5'-end-labeled template-strand (labeled using T4 polynucleotide kinase and [γ-^{32}P]ATP; 111 Bq/fmol) and 0.2 µM nontemplate-strand oligodeoxyribonucleotides corresponding to positions -100 to +50 of the *T. thermophilus rrn* (16S RNA; *33*), *T. thermophilus crtB* (*30*), *E. coli lacUV5* (*34*), *E. coli rrnB* P1 (*35*), and CC(-41.5) (*31*) promoters. For hydroxyl-radical DNA footprinting with *T. thermophilus* RNAP holoenzyme and RNAP holoenzyme derivatives, the sequence of template-strand positions -11 to +2 was altered to match the sequence of nontempate-strand positions -11 to +2, resulting in a pre-melted transcription bubble (see *36*).

Protein-DNA interaction assays: electrophoretic mobility shift assays

Electrophoretic mobility shift assays with the nucleic-acid scaffold for crystallization were performed in reaction mixtures containing (20 µl): 0 or 200 nM *T. thermophilus* TAP, 100 nM *T.*

thermophilus RNAP holoenzyme, 100 nM nucleic-acid scaffold, 20 mM Tris-HCl (pH 7.7), 0.1 M NaCl, and 1% glycerol. Reaction mixtures were incubated 15 min at 25°C, applied to 5% TBE precast polyacrylamide slab gels (BioRad, Inc.), electrophoresed in 90 mM Tris-borate (pH 8.0) and 0.2 mM EDTA, stained with SYBR Gold Nucleic Acid Stain (ThermoFisher, Inc.) according to the procedure of the manufacturer, and analyzed by x/y fluorescence scanning (Typhoon; GE Healthcare, Inc.).Electrophoretic mobility shift assays for analysis of effects of substitutions of σ^{70} were performed in reaction mixtures containing (20 µl): 200 nM *E. coli* RNAP holoenzyme or substituted RNAP holoenzyme derivative, 5 nM Cy5-labeled λP_R-P_{RMup} promoter DNA fragment, 30 mM HEPES-NaOH (pH 7.5), 0.1 M KCl, 1 mM dithiothreitol, and 50 µg/ml bovine serum albumin. Reaction mixtures were incubated 15 min at 25°C, supplemented with 1 µl 2 mg/ml heparin, incubated 1 min at 25°C, applied to 5% TBE precast polyacrylamide slab gels (BioRad, Inc.), electrophoresed in 90 mM Tris-borate (pH 8.0) and 0.2 mM EDTA, and analyzed by x/y fluorescence scanning (Typhoon; GE Healthcare, Inc.).

Protein-DNA interaction assays: hydroxyl-radical DNA footprinting

Hydroxyl-radical DNA footprinting with *T. thermophilus* RNAP holoenzyme and RNAP holoenzyme derivatives was performed as follows (see *35*, *37*): Reaction mixtures contained (100 µl): 0 or 100 nM *T. thermophilus* TAP, 100 nM *T. thermophilus* RNAP holoenzyme or RNAP holoenzyme derivative lacking αCTD [α(1-229)-RNAP], 1 nM *E. coli lacUV5*, *T. thermophilus rrn*, or *T. thermophilus crtB* promoter DNA fragment with pre-melted transcription bubble, 10 mM Tris (pH 7.9), 20 mM KCl, and 10 mM $MgCl_2$. Reaction mixtures were incubated 10 min at 37°C; supplemented with 1 µl 1 mg/ml heparin; incubated 1 min at 37°C; supplemented with 1 µl 0.1 M sodium ascorbate, 1 µl 1% H_2O_2, and 1 µl 1 mM $(NH4)_2Fe(SO_4)_2$ and 2 mM EDTA; and further incubated 2 min at 37°C. Reactions were terminated by adding 10 µl 0.1 M thiourea. Products were purified by ethanol precipitation, re-suspended in 5 µl loading buffer (10 mM EDTA, 0.02% bromophenol blue, 0.02% xylene cyanol, and 98% formamide), boiled 2 min, applied to 8% urea-polyacrylamide slab gels (19:1 acrylamide/bisacrylamide; *38*), electrophoresed in 90 mM Tris-borate (pH 8.0) and 0.2 mM EDTA, and analyzed by storage-phosphor scanning (Typhoon; GE Healthcare, Inc.).Hydroxyl-radical DNA footprinting with *E. coli* RNAP holoenzyme and RNAP holoenzyme derivatives was performed by the same procedure, but using 0 or 100 nM *E. coli* CAP, 100 nM *E. coli* RNAP holoenzyme or RNAP holoenzyme derivative lacking αCTD [α(1-235)-RNAP], and 1 nM *E. coli lacUV5*, *E. coli rrnB* P1, or CC(-41.5) promoter DNA fragment with fully complementary nontemplate and template strands, 0.2 mM cAMP (only in experiments with CC(-41.5)), and 0.5 mM ATP and 50 µM CTP (only in experiments with *rrnB* P1; see *35*).

Protein-protein interaction assays: fluorescence polarization assays of TAP-αCTD interaction

Equilibrium fluorescence polarization assays (*39*) were performed in a 96-well microplate format. Reaction mixtures contained (105 µl): 0-80 µM *T. thermophilus* TAP or TAP derivative, 100 nM fluorescein-labelled αCTD ([fluorescein-Cys311]αCTD), 50 mM glycine-NaOH (pH 8.5), 50 mM KCl, 18 mM $MgCl_2$, 0.1 mM EDTA, 5 mM dithiothreitol, and 50 µg/ml bovine serum albumin. Following incubation mixtures for 10 min at 25°C, fluorescence emission intensities were measured using a microplate reader (GENios Pro; TECAN, Inc; excitation wavelength = 485 nm; emission wavelength = 535 nm). Fluorescence polarization was calculated using:

$$P = (I_{VV} - I_{VH})/(I_{VV} + I_{VH}) \quad (1)$$

where I_{VV} and I_{VH} are fluorescence intensities with the excitation polarizer at the vertical position and the emission polarizer at, respectively, the vertical position and the horizontal position.

Equilibrium dissociation constants, K_D, were extracted by non-linear regression using the equation:

$$P = P_f + \{(P_b - P_f) \times [T] / (K_D + [T])\} \quad (2)$$

where P is the fluorescence polarization at a given concentration of TAP, P_f is the fluorescence polarization for free [fluorescein-Cys311]αCTD, P_b is the fluorescence polarization for bound [fluorescein-Cys311]αCTD, and [T] is the concentration of wild-type or substituted TAP.

Protein-protein interaction assays: fluorescence polarization assays of TAP-RNAP interaction

Equilibrium fluorescence polarization assays of TAP-RNAP interaction were performed analogously to fluorescence polarization assays of TAP-αCTD interaction, using 0-4 μM *T. thermophilus* RNAP holoenzyme or RNAP holoenzyme derivative and 100 nM fluorescein-labelled *T. thermophilus* TAP ([fluorescein-Cys133]TAP).

Transcription assays: scaffold transcription assays

Scaffold transcription assays were performed in reaction mixtures containing (10 μl): 40 nM *T. thermophilus* TAP, 100 nM *T. thermophilus* RNAP holoenzyme, 5 nM nucleic-acid scaffold, 50 mM glycine-NaOH (pH 8.5), 50 mM KCl, 18 mM $MgCl_2$, 0.1 mM EDTA, 5 mM dithiothreitol, and 50 μg/ml bovine serum albumin. Reaction mixtures were incubated 10 min at 25°C, supplemented with 0.15 μl 3.3 μM [α-^{32}P]CTP (100 Bq/fmol), and RNA synthesis was allowed to proceed for 15 min at 65°C. Reactions were terminated by adding 10 μl loading buffer (10 mM EDTA, 0.02% bromophenol blue, 0.02% xylene cyanol, and 98% formamide) and boiling for 2 min. Products were applied to 22% urea-polyacrylamide slab gels (19:1 acrylamide/bisacrylamide; *38*), electrophoresed in 90 mM Tris-borate (pH 8.0) and 0.2 mM EDTA, and analyzed by storage-phosphor scanning (Typhoon; GE Healthcare, Inc.).

Transcription assays: abortive initiation assays

Abortive initiation assays with *T. thermophilus* RNAP holoenzyme were performed in reaction mixtures containing (10 μl): 0 or 40 nM *T. thermophilus* TAP or TAP derivative, 100 nM *T. thermophilus* RNAP holoenzyme or RNAP holoenzyme derivative, 5 nM *T. thermophilus crtB* promoter DNA fragment, 50 mM glycine-NaOH (pH 8.5), 50 mM KCl, 18 mM $MgCl_2$, 0.1 mM EDTA, 5 mM dithiothreitol, and 50 μg/ml bovine serum albumin. Reaction mixtures were incubated 10 min at 25°C, supplemented with 0.5 μl 10 mM ApA (RiboMed, Inc.) and 0.15 μl 3.3 μM [α-^{32}P]GTP (100 Bq/fmol), and RNA synthesis was allowed to proceed for 15 min at 65°C. Reactions were terminated and products were analyzed as described above for scaffold transcription assays.Abortive initiation assays with *E. coli* RNAP holoenzyme were performed in reaction mixtures containing (10 μl): 0 or 10 nM *E. coli* CAP or CAP derivative, 0.2 mM cAMP, 40 nM *E. coli* RNAP holoenzyme or RNAP holoenzyme derivative, 0.1 nM CC(-41.5) promoter DNA fragment, 50 mM Tris-HCl (pH 8.0), 100 mM KCl, 10 mM $MgCl_2$, 5 mM dithiothreitol, and 50 μg/ml bovine serum albumin. Reaction mixtures were incubated 10 min at 25°C, supplemented with 0.5 μl 10 mM ApU (RiboMed, Inc.) and 0.075 μl 6.7 μM [α-^{32}P]UTP (100 Bq/fmol), and RNA synthesis was allowed to proceed for 15 min at 30°C. Reactions were terminated and products were analyzed as described above for scaffold transcription assays.

Transcription assays: abortive initiation kinetics assays

Fluorescence-detected abortive initiation assays were performed by a variation of the method of *40*. Reaction mixtures contained (500 μl): 40 nM *T. thermophilus* TAP or TAP derivative, 0, 4, 5, 7, 10, 13, 17, or 25 nM *T. thermophilus* RNAP holoenzyme, 1 nM *T. thermophilus crtB* promoter DNA fragment, 0.5 mM ApA (RiboMed, Inc.), 1 mM GTP, and 50 μM γ-(5-aminonapthylenesulphonate)-UTP [(γ-AmNS)UTP; Jena Bioscience, Inc.], 50 mM glycine-NaOH (pH 8.5), 50 mM KCl, 18 mM $MgCl_2$, 0.1 mM EDTA, 5 mM DTT, and 50 μg/ml bovine serum albumin. Reaction components except the promoter DNA fragment were pre-equilibrated for 10 min at 65°C in sub-micro fluorometer cuvettes (Starna Cells, Inc.). Reactions were initiated by addition of the promoter DNA fragment, and fluorescence emission intensity was monitored for 30-60 min at 65°C [1 measurement per second; excitation wavelength = 360 nm; emission wavelength = 500 nm; excitation and emission slit widths = 2

nm; QuantaMaster QM1 spectrofluorometer (PTI, Inc.)]. Time constants (τ_{obs}), binding constants for formation of RNAP-promoter closed complex (K_B), and rate constants for isomerization of RNAP-promoter closed complex to RNAP-promoter open complex (k_f) were extracted as in *41-42*.

Structure determination: assembly of transcription activation complexes

Transcription activation complexes for crystallization were prepared by mixing 1.5 ml 3.6 μM *T. thermophilus* TAP (in 20 mM Tris-HCl, pH 7.7, 0.5 M NaCl, and 5% glycerol), 200 μl 14 μM *T. thermophilus* holoenzyme (in 20 mM Tris-HCl, pH 7.7, 0.1 M NaCl, and 1% glycerol), 12 μl 0.28 mM nucleic-acid scaffold (in 5 mM Tris-HCl, pH 7.7, 0.2 M NaCl, and 10 mM $MgCl_2$), and 6 ml 20 mM Tris-HCl, pH 7.7, and incubating 1 h at 4°C. Complexes were concentrated to 160 μl using Amicon Ultra-4 centrifugal ultrafilters (10 kDa MWCO; Millipore, Inc.) immediately before crystallization.

Structure determination: crystallization and cryo-cooling

Robotic crystallization trials were performed using a Gryphon liquid handling system (Art Robbins Instruments, Inc.), commercial screening solutions (Emerald Biosystems, Inc.; Hampton Research, Inc.; and Qiagen, Inc.), and the sitting-drop vapor diffusion technique (drop: 0.2 μl transcription activation complex plus 0.2 μl screening solution; reservoir: 60 μl screening solution; 22°C). 900 conditions were screened. Under several conditions, crystals appeared within 1 week. Conditions were optimized using the hanging-drop vapor-diffusion technique at 22°C. The optimized conditions (drop: 1 μl transcription activation complex plus 1 μl 0.1 M HEPES-NaOH, pH 7.6, 0.1 M $MgCl_2$, and 6% PEG4000; reservoir: 500 μl 0.1 M HEPES-NaOH, pH 7.6, 0.1 M $MgCl_2$, and 6% PEG4000; 22°C) yielded diffraction-quality, plate-like crystals with dimensions of 0.2 mm x 0.2 mm x 0.05 mm in 1 week (Fig. S1E). Crystals were transferred to reservoir solution containing 20% (v/v) (2R,3R)-(-)-2,3-butanediol (Sigma-Aldrich, Inc.) and flash-cooled with liquid nitrogen.

Structure determination: data collection and reduction

Diffraction data were collected from cryo-cooled crystals at Brookhaven National Laboratory beamline X25. Data were processed using HKL2000 (*43*). The resolution cut-off criteria were: (i) $I/\sigma > 1.5$, (ii) $R_{merge} < 1$, and (iii) completeness > 90%.

Structure determination: structure solution and refinement

The structure was solved by molecular replacement with Molrep (*44*) using the structure of *T. thermophilus* RPo (PDB 4G7H) as the search model. A single dataset from a single crystal was used for refinement, and R_{free} test reflections were kept constant through the refinement. Early-stage refinement included rigid-body refinement of each of the two RNAP molecules in the asymmetric unit, followed by rigid-body refinement of each subunit of each RNAP molecule, followed by rigid-body refinement of 40 domains of each RNAP molecule. Electron density for TAP, αCTD, and nucleic acids was unambiguous, but was not included in models in early-stage refinement. Cycles of iterative model building with Coot (*45*) and refinement with Phenix (*46*) then were performed. A crystal structure of TAP (PDB 3B02) and an NMR structure of αCTD (PDB 1DOQ) were fitted to electron density for TAP and αCTD by manual fitting followed by rigid-body refinement. The final model was generated by XYZ-coordinate refinement with non-crystallographic-symmetry and secondary-structure restraints, followed by group B-factor refinement. Electron-density maps showed unambiguous density for 195 TAP residues, 3,132 RNAP residues, 346 σ residues, DNA nontemplate-strand nucleotides -54 to +12, DNA template-strand nucleotides -54 to +12, and UpCpGpA (Fig. S2). The final model, refined to R_{work} and R_{free} of 0.24 and 0.28, respectively, was deposited in the PDB with accession code 5I2D (Table S1).

Positions of protein backbone atoms and protein sidechain Cβ atoms are well-defined in electron-density maps (Fig. S2). Positions of protein sidechain atoms beyond Cβ are well-defined for some residues (Fig. S2E-F), but are not well-defined for other residues, particularly solvent-exposed residues (Fig. S2E-F). In figure panels showing atom representations of protein residues, only protein Cα atoms are shown (as spheres with radius = 3.4 Å).

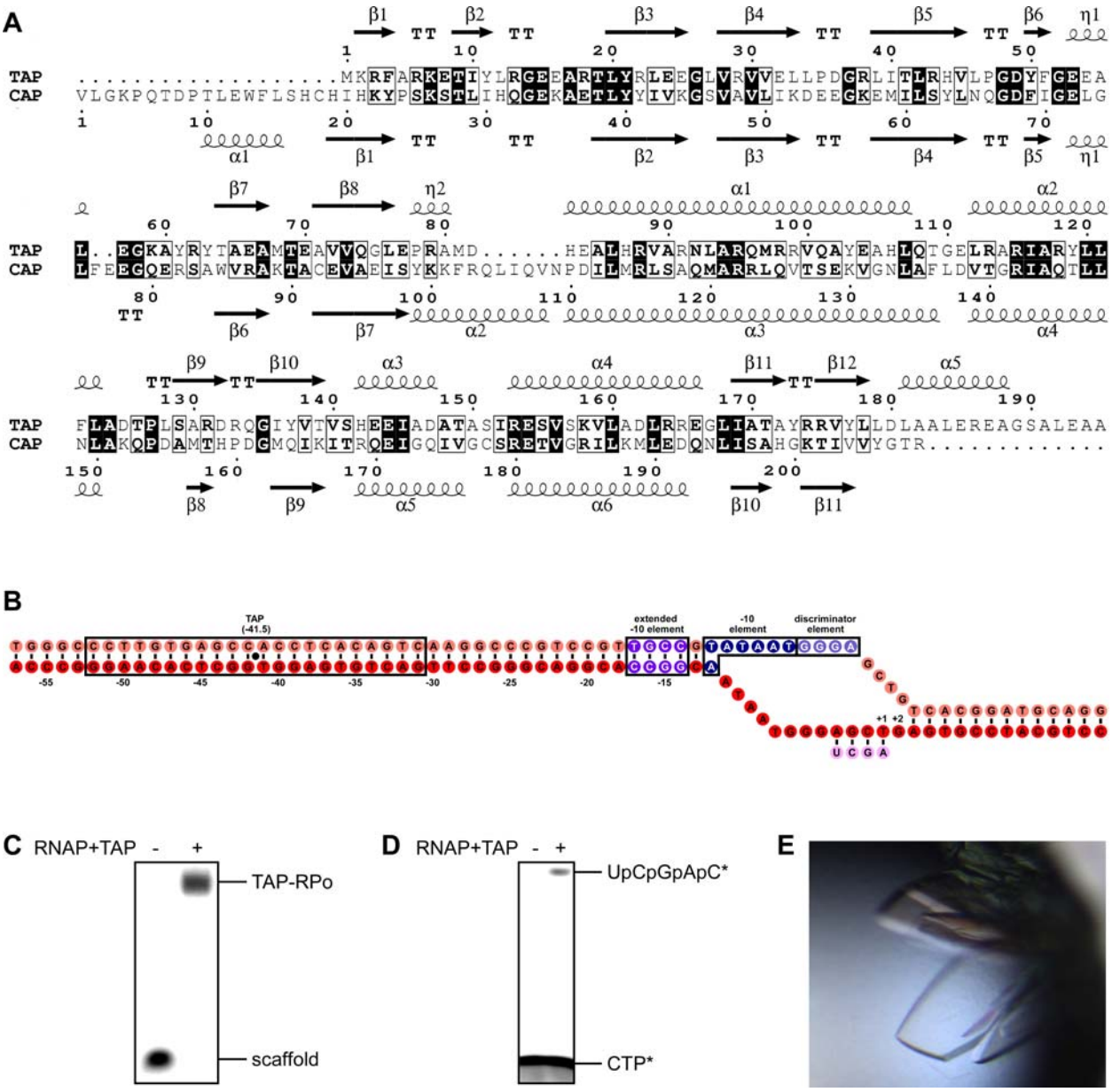

Fig. S1. Crystal structure of TAP-RPo: TAP, nucleic-acid scaffold, and crystallization.
(A) Sequences of TAP and CAP (*5*, *47-48*).
(B) Sequence of nucleic-acid scaffold. Colors as in Fig. 1A.
(C) Formation of TAP-RPo with nucleic-acid scaffold.
(D) Transcription initiation with nucleic-acid scaffold.
(E) TAP-RPo crystals.

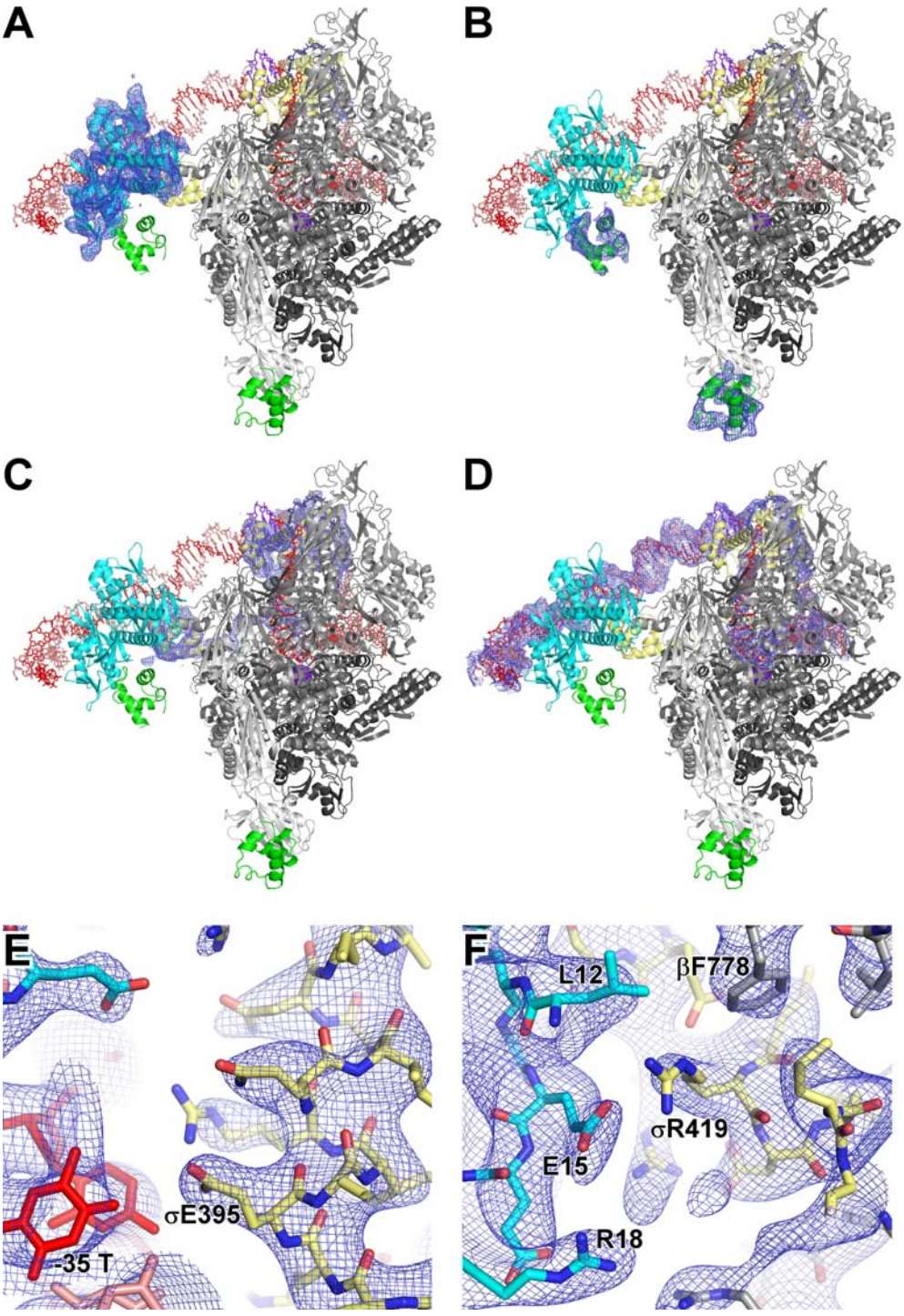

Fig. S2. Crystal structure of TAP-RPo: electron density maps.
(A-D) Experimental electron density for TAP (A), αCTD (B), σ (C), and nucleic acids (D) (blue mesh, F_o-F_c omit map, contoured at 2.5σ). View orientation, rendering and colors as in Fig. 1B.
(E-F) Experimental electron density for representative protein-DNA interaction (protein-DNA interaction of σR4 with -35-element; E) and representative protein-protein interaction (protein-protein interaction of TAP AR3 with σR4 and β flap tip; F) (blue mesh, $2F_o$-F_c map, contoured at 1.0σ). Cyan, TAP carbon atoms; yellow, σR4 carbon atoms; gray, β carbon atoms; blue, TAP, σR4, and β nitrogen atoms; red, TAP, σR4, and β oxygen atoms; pink, DNA nontemplate-strand atoms, red, DNA template-strand atoms.

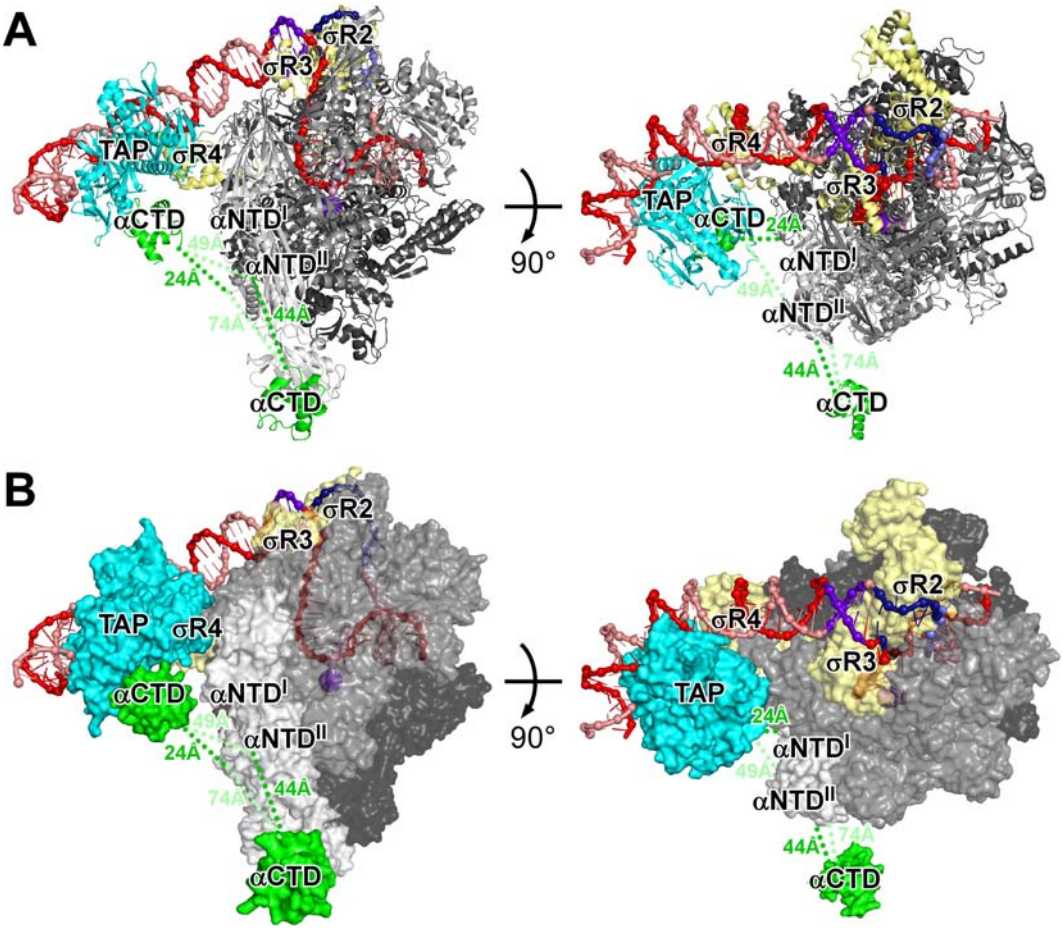

Fig. S3. Crystal structure of TAP-RPo: linkages between αCTD and αNTD.
(A-B) Structure of TAP-RPo showing αCTD-αNTD distances (green and light green dotted lines; view orientations, rendering, and other colors as in Fig. 1B-C). The 24-residue linker between each αCTD and its corresponding αNTD is disordered, indicating that each linker adopts multiple conformations. The N-terminus of the αCTD that interacts with TAP is 24 Å from the C-terminus of αNTD^{I} (the αNTD that interacts with β) and 49 Å from the C-terminus of αNTD^{II} (the αNTD that interacts with β'). The N-terminus of the other αCTD is 74 Å from the C-terminus of αNTD^{I} and 44 Å from the C-terminus of αNTD^{II}. All of these distances are within the range of distances that could be spanned by a 24-residue linker (up to ~90 Å), but the distance between the N-terminus of the second αCTD and the C-terminus of αNTD^{I} is at the upper edge of the range of distances. We infer that each αCTD potentially could be linked to either αNTD^{I} or αNTD^{II} (green and light green dotted lines), but that, preferably, the αCTD that interacts with TAP is linked to αNTD^{I} and the other αCTD is linked to αNTD^{II} (green dotted lines; Fig. 1B-C).
All other instances of αCTD within the crystal lattice (e.g., αCTD^{tan}; Fig. S4) are too distant from αNTD^{I} and αNTD^{II} to be connected through a 24-residue linker (sterically accessible distances ≥95 Å).

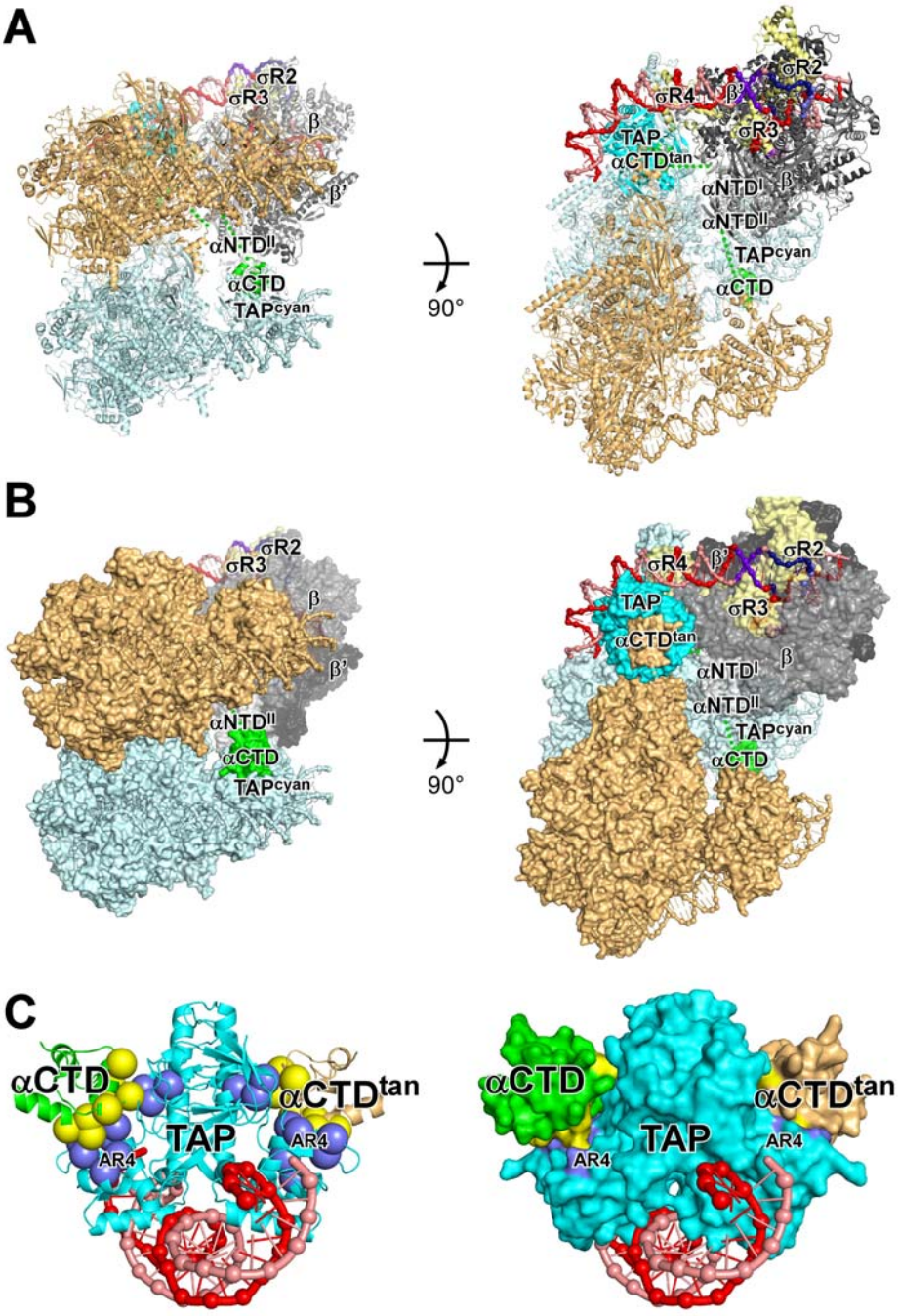

Fig. S4. Crystal structure of TAP-RPo: lattice interactions involving αCTD.
(A-B) Portion of crystal lattice comprising TAP-RPo (colors as in Fig. 1B-C) and two adjacent molecules of TAP-RPo (colored tan and cyan) (view orientations and rendering as in Fig. 1B-C). The second αCTD of TAP-RPo interacts with the unoccupied face of the TAP dimer in the cyan adjacent molecule of TAP-RPo (TAP^{cyan}). The second αCTD of the tan adjacent molecule of TAP-RPo interacts with the unoccupied face of the TAP dimer of TAP-RPo (αCTD^{tan}).
(C) Portion of crystal lattice comprising TAP and αCTD of TAP-RPo (colors as in Fig. 4A) and the second αCTD of tan adjacent molecule of TAP-RPo (αCTD^{tan}) (colored tan) (view orientations and rendering as in Fig. 4A). The interactions between TAP and αCTD of TAP-RPo and the interactions between TAP of TAP-RPo and αCTD^{tan} involve opposite, two-fold-symmetry-related faces of TAP dimer and identical, two-fold-symmetry-related contacts.

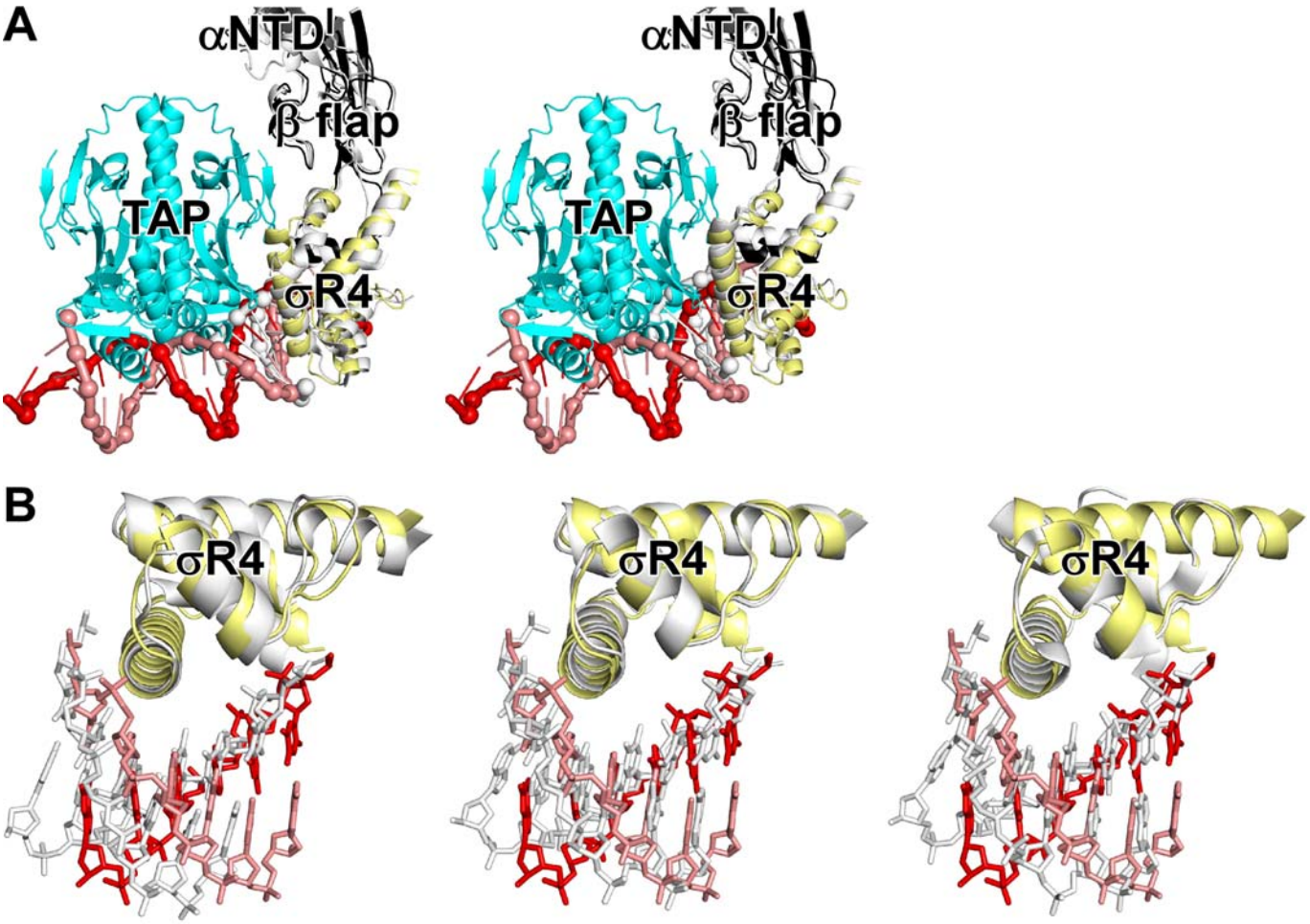

Fig. S5. Comparison of σR4-DNA interactions in TAP-RPo to σR4-DNA interactions in RPo.
(A) Superimposition of upstream portion of TAP-RPo (colors as in Fig. 1B-C) on corresponding portion of RPo of *8* (gray; left subpanel) and *9-10* (gray; right subpanel) (structures superimposed using RNAP β atoms).
(B) Superimposition of σR4-DNA in TAP-RPo (colors as in Fig. 1B-C) on σR4-DNA of *8* (gray; left subpanel), *9-10*, (gray; middle subpanel), and *49* (gray; right subpanel) (structures superimposed using σR4 atoms).

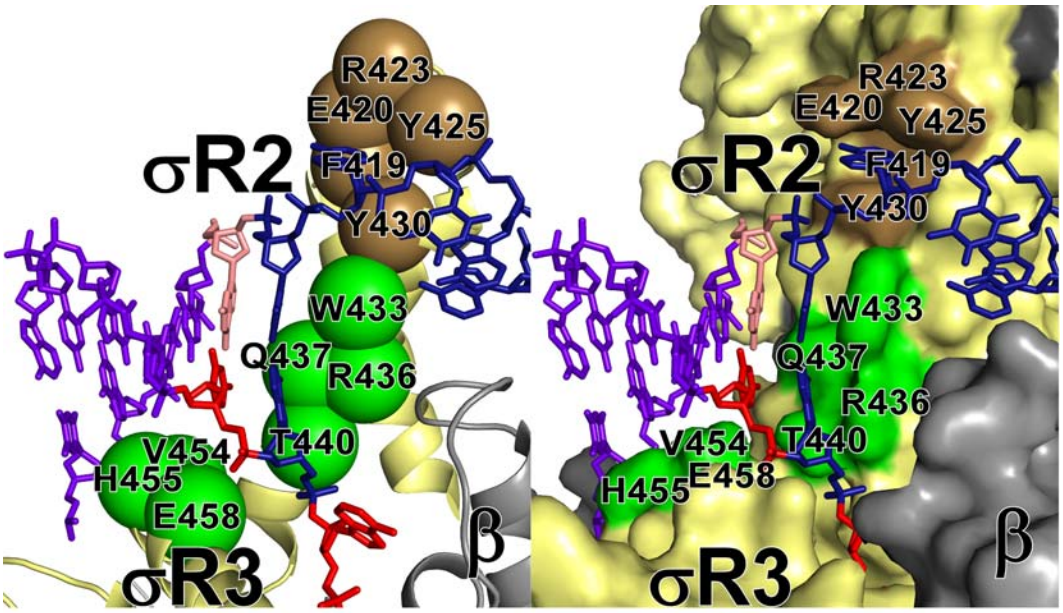

Fig. S6. Interactions of RNAP holoenzyme with promoter upstream fork junction.
Left subpanel, ribbon representation; right subpanel, surface representations. Colors as in Figs. 1B-C and 2. Residues numbered as in *E. coli* σ^{70}. The view orientation highlights the binding of the nontemplate-strand -11 base within a pocket formed by σ residues F419, E420, R423, Y425, and Y430 and the binding of the template-strand -11 base within a narrow channel formed by σ and β residues.

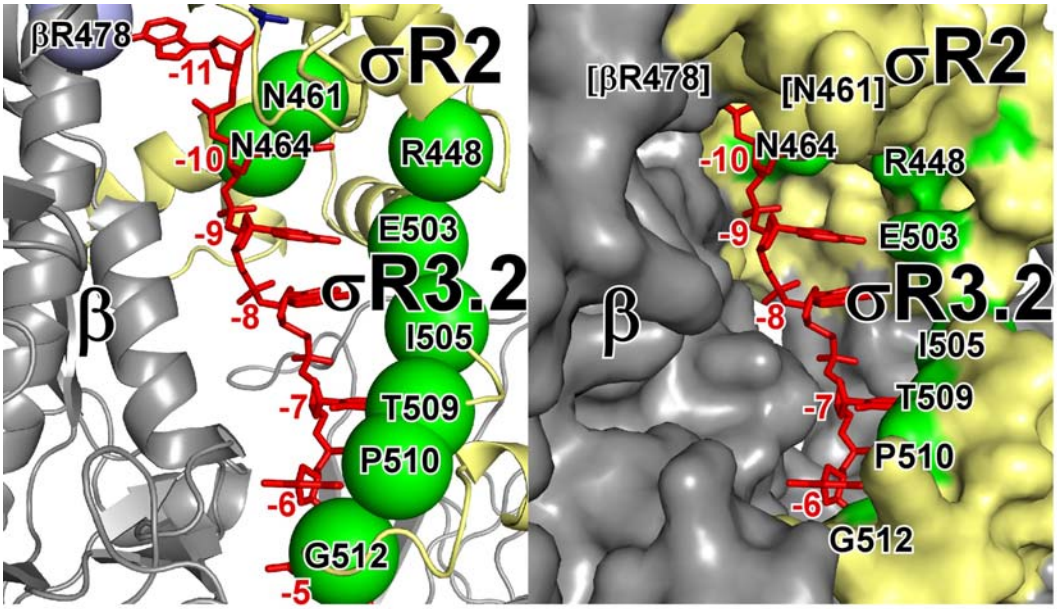

Fig. S7. Interactions of RNAP holoenzyme with template strand of transcription bubble.
Left subpanel, ribbon representation; right subpanel, surface representation. Light blue, RNAP core residue proposed to make direct contact with template-strand base -11; green, σR2 and σR3.2 residues proposed to make direct contacts with template-strand bases -10 through -5; other colors as in Fig. 1B-C. Residues numbered as in *E. coli* RNAP and σ^{70}.
The overall path of template-strand nucleotides -11 to -5 is the same in TAP-RPo as in RPo (*8-10*). The resolutions of crystal structures of TAP-RPo and RPo (4.0-5.5 Å; Fig. S2B; *8-10*) are insufficient to define unambiguously the orientations and interactions of template-strand ssDNA nucleotides -11 to -5. We propose a nucleotide orientation that places nucleotide phosphates in contact with RNAP core and places nucleotide bases in contact with σR2 and σR3.2. Two lines of evidence suggest that the nucleotide orientation proposed here is more likely to be correct than the ~100-180° different nucleotide orientations proposed in *8-10*: (i) superior electrostatic complementarity (4 Å vs. up to 5 Å mean distance between nucleotide phosphates and closest positively charged protein residues), and (ii) superior match to the nucleotide orientation in the 2.5 Å resolution crystal structure of the transcription elongation complex (3 Å vs. up to 5 Å root mean square deviation in phosphate positions for closest nucleotides in transcription elongation complex of *50*). The nucleotide orientation proposed here predicts direct interactions between template-strand bases -11 through -5, raising the possibility that some or all of template-strand positions -11 through -5 may contribute to sequence-specific promoter recognition.

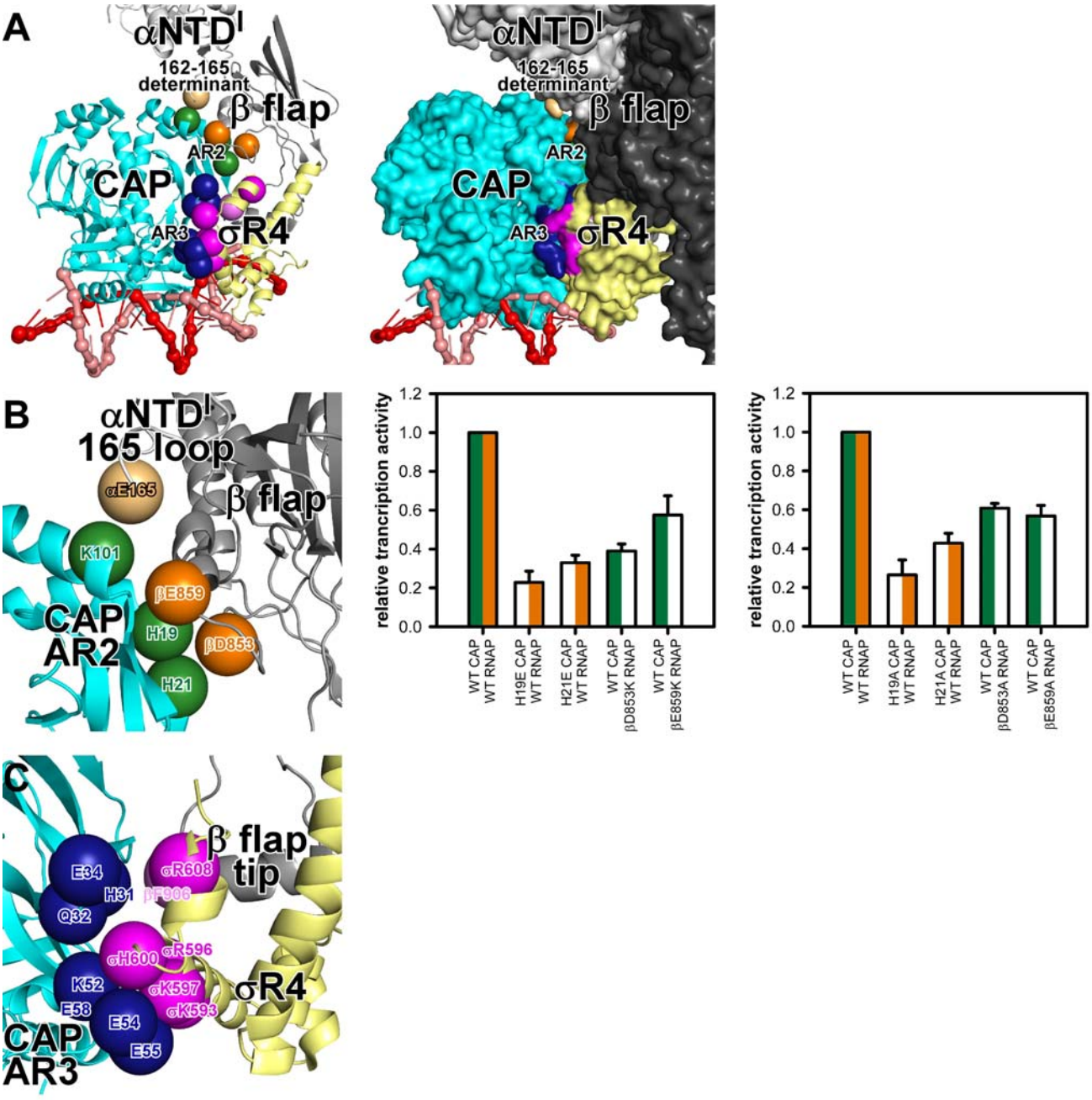

Fig. S8. Homology model of *E. coli* CAP-RPo.
(A) Interaction between AR2 and AR3 and RNAP holoenzyme in homology model of *E. coli* CAP-RPo constructed based on crystal structures of TAP-RPo, *E. coli* CAP-DNA (*6, 51*) and *E. coli* RNAP σ^{70} holoenzyme (*52-54*). Light orange, residue of the *E. coli* αNTD^{I} species-specific insertion ("162-165 determinant"; *1-2, 13*) inferred to make direct contact with CAP AR2. View orientations, rendering, and other colors as in Fig. 3A.
(B) AR2 interactions (left) and effects on CAP-dependent transcription of charge-reversal substitutions (middle) and Ala substitutions (right) of proposed contact residues (colored/colored bars, wild-type CAP and wild-type RNAP; uncolored/colored bars, mutant CAP and wild-type RNAP; colored/uncolored bars, wild-type CAP and mutant RNAP).
(C) AR3 interactions.

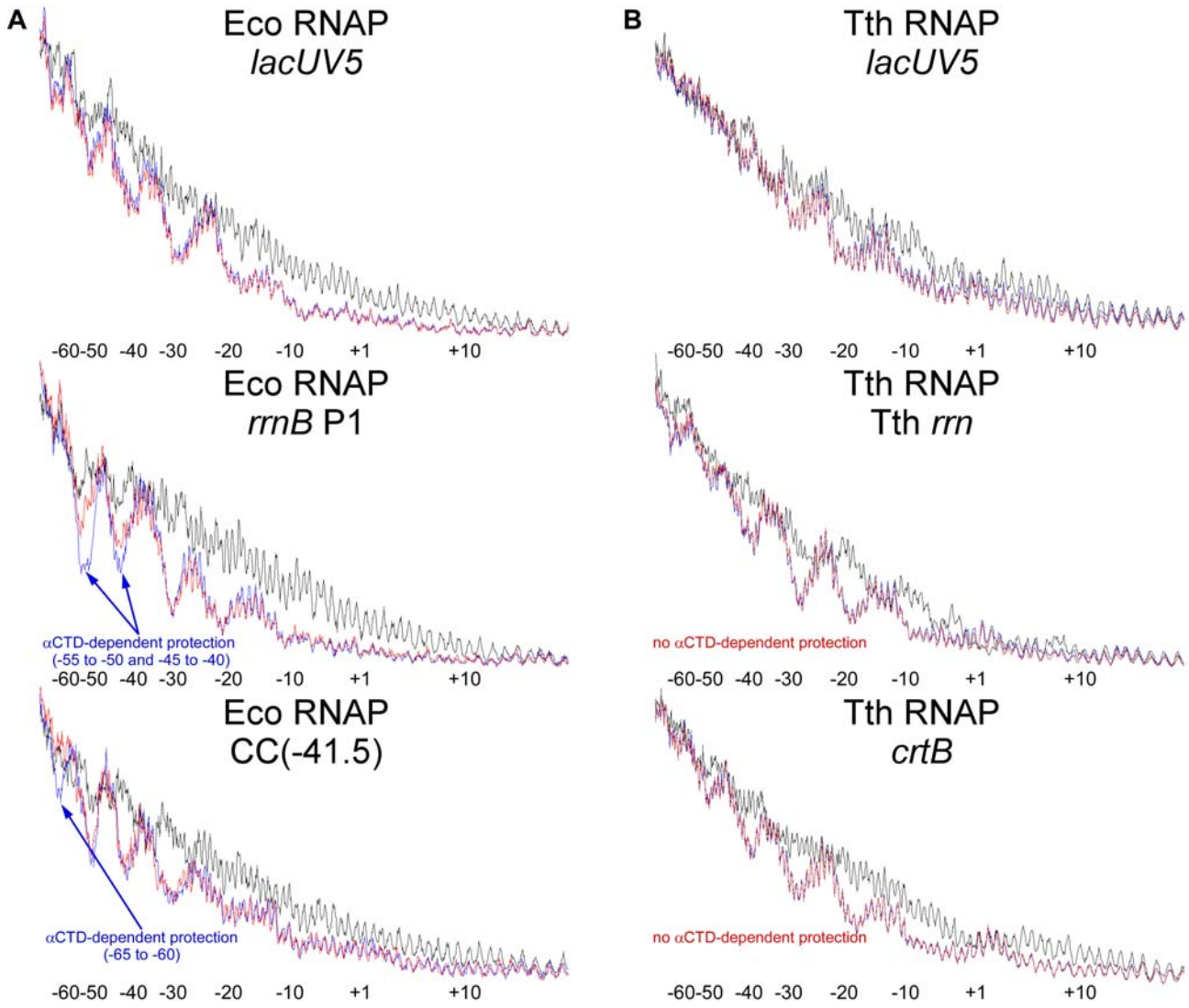

hydroxyl-radical DNA footprinting.
(A) Hydroxyl-radical DNA footprints of *E. coli* RPo at a simple, UP-element-independent, activator-independent promoter (top; *lacUV5*), an *E. coli* ribosomal RNA promoter (middle; *rrnB* P1), and a Class II CAP-dependent promoter (bottom; CC(-41.5)). Black, no RNAP; blue, *E. coli* RNAP holoenzyme; red, *E. coli* RNAP holoenzyme derivative lacking αCTD (*E. coli* α(1-235)-RNAP). αCTD-dependent protection is observed immediately upstream of -35-element in RPo at the *E. coli* ribosomal RNA promoter and immediately upstream of the DNA site for CAP in RPo at the *E. coli C*lass II CAP-dependent promoter (see *35, 37*).
(B) Hydroxyl-radical DNA footprints of *T. thermophilus* RPo at a simple, UP-element-independent, activator-independent promoter (top; *lacUV5*), a *T. thermophilus* ribosomal RNA promoter (middle; *rrn*), and a *T. thermophilus* Class II TAP-dependent promoter (bottom; *crtB*). Colors as in A. No αCTD-dependent protection is observed upstream of the -35 element in RPo at the *T. thermophilus* ribosomal RNA promoter, and no protection is observed upstream of the DNA site for TAP in RPo at the *T. thermophilus* Class II TAP-dependent promoter.

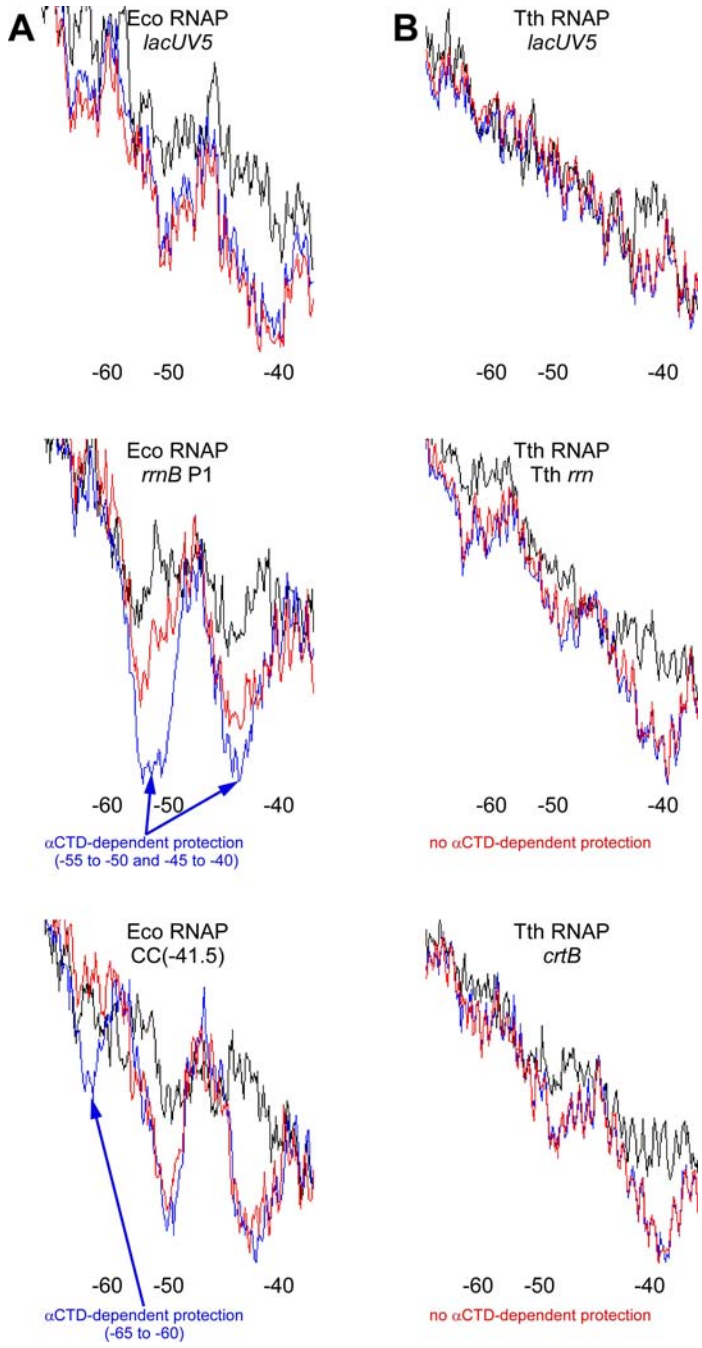

Fig. S10. Differences in αCTD function in *E. coli* and *T. thermophilus*: hydroxyl-radical DNA footprinting.
Expanded view of hydroxyl-radical DNA footprints for promoter positions -70 through -35 (see Fig. S9).

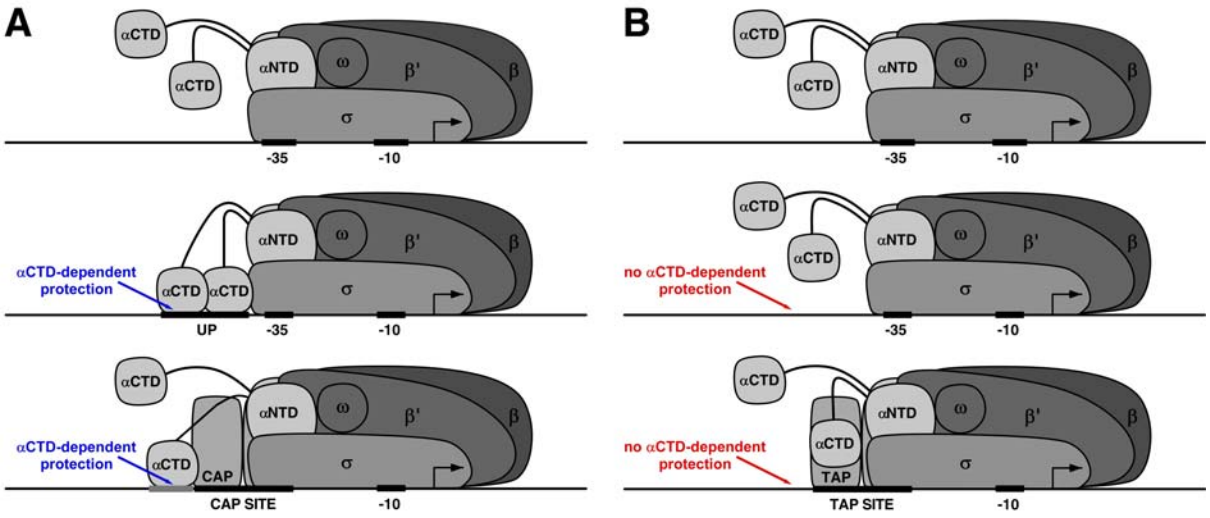

Fig. S11. Differences in αCTD function in *E. coli* and *T. thermophilus* RPo: summary
(A) Schematic models of *E. coli* RPo at a simple, UP-element-independent, activator-independent promoter (top; e.g., *lacUV5*), an *E. coli* ribosomal RNA promoter (middle; e.g., *rrnB* P1), and an *E. coli* Class II activator-dependent promoter (bottom; e.g., CC(-41.5)) (Figs. S9-S10; *1-3, 35, 37*). Horizontal lines, promoter DNA; black bars, sequence-specific protein-DNA interactions between σ and -35 and -10 elements, αCTD and A/T-rich UP-element DNA, and activator and activator site; gray bar, activator-dependent protein-DNA interaction between αCTD and DNA immediately upstream of activator site; arrows, transcription start sites; very light, light, medium, and dark gray, RNAP α, σ, β' and ω, and β subunits; curved lines, linkers connecting αNTD and αCTD. Both copies of αCTD in *E. coli* RNAP make sequence-specific protein-DNA interactions with A/T-rich UP-element DNA at the ribosomal RNA promoter. One copy of αCTD in *E. coli* RNAP makes protein-protein interactions with the activator and activator-dependent protein-DNA interactions with adjacent DNA at the Class II activator-dependent promoter.
For simplicity, αCTD not interacting with A/T-rich UP-element DNA or an activator is shown making no interactions. Protein-DNA crosslinking results indicate that αCTD not interacting with A/T-rich UP-element DNA or an activator makes weak, transient non-sequence-specific protein-DNA interactions with upstream DNA (*55*).
(B) Schematic models of *T. thermophilus* RPo at a simple promoter, UP-element-independent, activator-independent (top ; *lacUV5*), a *T. thermophilus* ribosomal RNA promoter (middle; *rrn*), and a *T. thermophilus* Class II activator-dependent promoter (bottom; *crtB*) (Figs. 1B-C, S9-S10). Symbols and colors as in A. One copy of αCTD in *T. thermophilus* RNAP interacts with the activator, but not adjacent DNA, at the Class II activator-dependent promoter. No copy of αCTD in *T. thermophilus* RNAP makes sequence-specific or activator-dependent protein-DNA interactions at any of the three promoters.
We speculate that the different, more restricted, role of αCTD in *T. thermophilus* may be an adaptation to growth of *T. thermophilus* at high temperatures, for which low-melting-temperature A/T-rich, UP-element-like DNA sequences may be unfavorable.

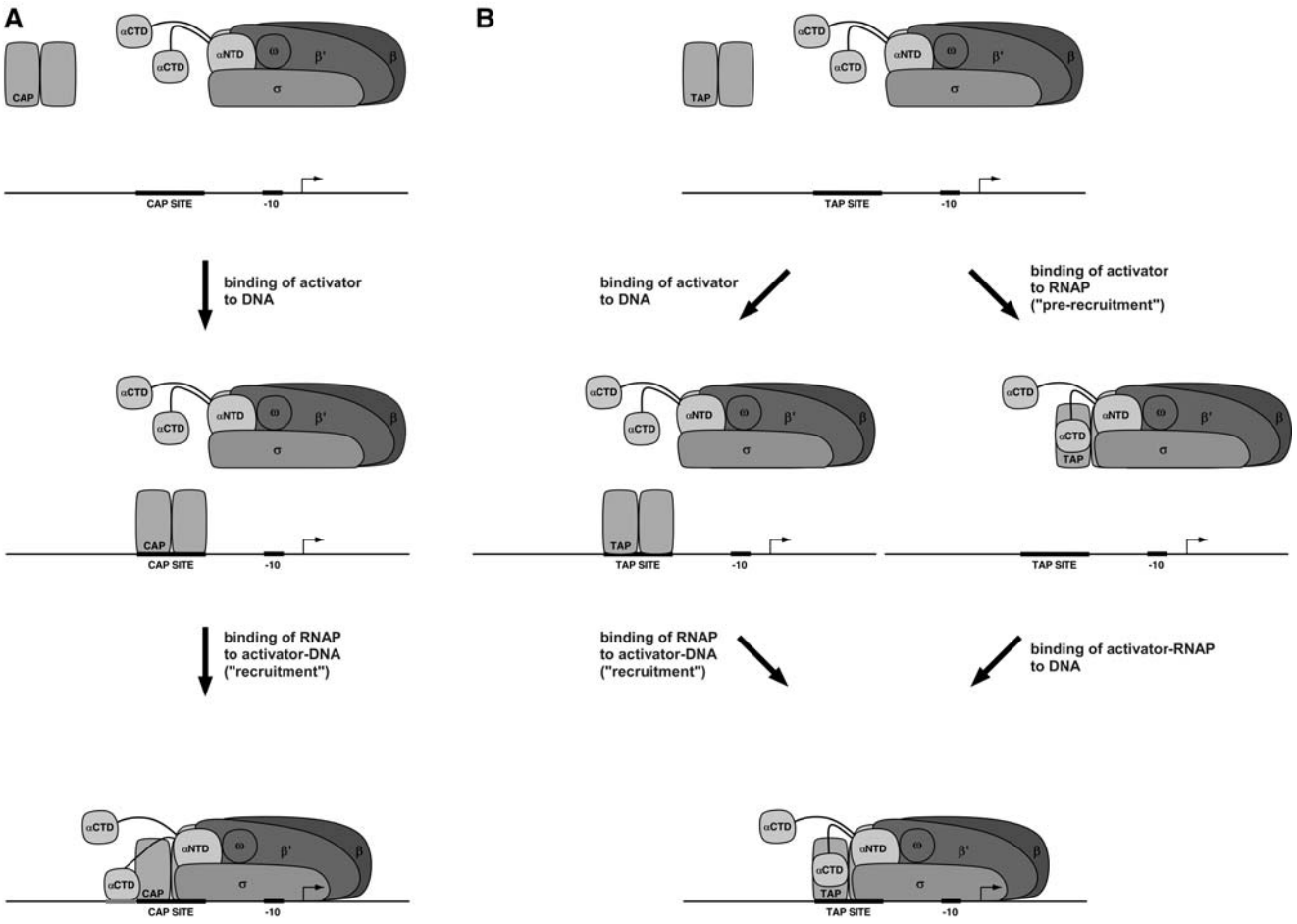

Fig. S12. Differences in αCTD function in *E. coli* and *T. thermophilus* RPo: recruitment and pre-recruitment.
(A) Pathway for formation of a transcription activation complex at an *E. coli* Class II CAP-dependent promoter. CAP binds to DNA and "recruits" RNAP holoenzyme to DNA. The bottom arrow denotes both binding of RNAP holoenzyme to promoter DNA to form RPc and isomerization of RPc to form RPo.
(B) Pathway for formation of a transcription activation complex at a *T. thermophilus* Class II TAP-dependent promoter. Because *T. thermophilus* TAP, unlike *E. coli* CAP, can bind tightly to RNAP holoenzyme in the absence of DNA (Fig. 4C, right; K_D = 6 μM) TAP in principle can access both a recruitment pathway, in which TAP first binds to DNA and then binds to RNAP holoenzyme, and a pre-recruitment pathway, in which TAP first binds to RNAP holoenzyme and then binds to DNA. The left bottom arrow denotes both the binding of RNAP holoenzyme to promoter DNA to form RPc and the isomerization of RPc to form RPo; the right bottom arrow denotes both the binding of the TAP-RNAP holoenzyme complex to promoter DNA to form RPc and the isomerization of RPc to form RPo.
For simplicity, the interactions between TAP and RNAP holoenzyme in the TAP-RNAP holoenzyme complex in the absence of DNA are drawn as being the same as the interactions between TAP and RNAP holoenzyme in TAP-RPo. Fluorescence-polarization results indicate that TAP AR2 and AR3 do not functionally interact with RNAP holoenzyme in the TAP-RNAP holoenzyme complex in the absence of DNA (Fig 4C, right), indicating that the orientation of TAP relative to RNAP holoenzyme in the TAP-RNAP holoenzyme complex in the absence of DNA may differ from the orientation in TAP-RPo.
Fluorescence polarization results further indicate that TAP interacts more strongly with RNAP holoenzyme in the absence of DNA than with αCTD in the absence of DNA (K_D = 6 μM in Fig. 4C, right vs. K_D = 50 μM in Fig. 4C, left), indicating that TAP may interact with both copies of αCTD, rather than just one, in RNAP holoenzyme in the TAP-RNAP holoenzyme complex in the absence of DNA.

Table S1. Structure data collection and refinement statistics.

data collection	
space group	$P2_1$
cell dimensions	
a, b, c (Å)	171.5, 105.4, 374.6
α, β, γ (°)	90.0, 102.4, 90.0
resolution (Å)	50.00-4.40 (4.48-4.40)*
number of unique reflections	81823
R_{meas}	0.204 (0.782)
R_{pim}	0.081 (0.371)
$CC_{1/2}$ (%)	91.4 (74.9)
I/σI	8.2 (1.6)
completeness (%)	98.7 (93.9)
redundancy	5.9 (3.9)
refinement	
resolution (Å)	49.31-4.41 (4.52-4.41)
number of unique reflections	71660
number of test reflections	1794
R_{work}/R_{free}	0.24/0.28 (0.34/0.38)
number of atoms	
Protein	66874
ligand/ion	6
Wilson B-factor ($Å^2$)	156.7
average B-factors ($Å^2$)	
Protein	101.0
ligand/ion	41.7
root-mean-square deviations	
bond lengths (Å)	0.003
bond angles (°)	0.66
MolProbity statistics	
clash score	11.68
rotamer outliers (%)	6.2
Cβ outliers (%)	0.0
Ramachandran Plot	
favored (%)	98.0
outliers (%)	0.0

*Highest resolution shell in parentheses.

References

1. S. Busby, R.H. Ebright, Transcription activation by catabolite activator protein (CAP). *J. Mol. Biol.* **293**, 199 (1999).
2. C. Lawson , D. Swigon, K. Murakami, S. Darst, H. Berman, R.H. Ebright, Catabolite activator protein (CAP): DNA binding and transcription activation. *Curr. Opin. Structl. Biol.* **14**, 10 (2004).
3. K. Decker, D. Hinton, Transcription regulation at the core: similarities among bacterial, archaeal, and eukaryotic RNA polymerases. *Annu. Rev. Microbiol.* **67**, 113 (Jun 13, 2013).
4. B. Hudson, J. Quispe, S. Lara-González, Y. Kim, H. Berman, E. Arnold, *et al*., Three-dimensional EM structure of an intact activator-dependent transcription initiation complex. *Proc. Natl. Acad. Sci. USA* **106**, 19830 (2009).
5. Y. Agari, S. Kuramitsu, A. Shinkai, X-ray crystal structure of TTHB099, a CRP/FNR superfamily transcriptional regulator from *Thermus thermophilus* HB8, reveals a DNA-binding protein with no required allosteric effector molecule. *Proteins* **80**, 1490 (2012).
6. S. Schultz, G. Shields, T. Steitz, Crystal structure of a CAP-DNA complex: the DNA is bent by 90°. *Science* **253**, 1001 (1991).
7. Y. Zhang, Y. Feng, S. Chatterjee, S. Tuske, M. Ho, E. Arnold, *et al.*, Structural basis of transcription initiation. *Science* **338**, 1076 (2012).
8. Y. Zuo, T. Steitz, Crystal structures of the *E. coli* transcription initiation complexes with a complete bubble. *Mol. Cell* **58**, 534 (2015).
9. B. Bae, A. Feklistov, A. Lass-Napiorkowska, R. Landick, S. Darst, Structure of a bacterial RNA polymerase holoenzyme open promoter complex. *eLife* **4**, 4:e08504 (2015).
10. B. Bae, J. Chen, E. Davis, K. Leon, S. Darst, E. Campbell, CarD uses a minor groove wedge mechanism to stabilize the RNA polymerase open promoter complex. *eLife* **4**, e08505 (2015).
11. V. Rhodius, D. West, C. Webster, S. Busby, N. Savery, Transcription activation at Class II CRP-dependent promoters: the role of different activating regions. *Nucl. Acids Res.* **25**, 326 (1997).
12. C. Chan, M. Lonetto, C. Gross, Sigma domain structure. *Structure* **4**, 1235 (1996).
13. W. Niu, Y. Kim, G. Tau, T. Heyduk, R.H. Ebright, Transcription activation at Class II CAP-dependent promoters: two interactions between CAP and RNA polymerase. *Cell* **87**, 1123 (1996).
14. M. Lonetto , V. Rhodius, K. Lamberg, P. Kiley, S. Busby, C. Gross, Identification of a contact site for different transcription activators in region 4 of the *Escherichia coli* RNA polymerase σ^{70} subunit. *J. Mol. Biol.* **284**, 1353 (1998).
15. V. Rhodius, J. Busby, Interactions between activating region 3 of the *Escherichia coli* cyclic AMP receptor protein and region 4 of the RNA polymerase σ^{70} subunit: application of suppression genetics. *J. Mol. Biol.* **299**, 311 (2000).
16. M. Zafar, I. Shah, R. Wolf, Protein-protein interactions between σ^{70} region 4 of RNA polymerase and *Escherichia coli* SoxS, a transcription activator that functions by the prerecruitment mechanism. *J. Mol. Biol.* **401**, 13 (2010).
17. M. Patrick, P. Dennis, M. Ehrenberg, H. Bremer, Free RNA polymerase in *Escherichia coli*. *Biochimie* **119**, 80 (2015).
18. M. Ptashne, A. Gann, Transcriptional activation by recruitment. *Nature* **386**, 569 (1997).
19. S. Roy, S. Garges, S. Adhya, Activation and repression of transcription by differential contact: two sides of a coin. *J. Biol. Chem*. **273**, 14059 (1998).
20. S. Dove, F. Huang, A. Hochschild, Mechanism for a transcriptional activator that works at the isomerization step. *Proc. Natl. Acad. Sci. USA* **97**, 13215 (2000).
21. J. Wickstrum, S. Egan, Ni++-Affinity purification of untagged cAMP receptor protein. *Biotechniques* **33**, 728 (2002).
22. A. Kapanidis, Y. Ebright, R.H. Ebright, Site-specific incorporation of fluorescent probes into protein: hexahistidine-tag-mediated fluorescent labeling using (Ni2+:nitrilotriacetic acid)n-fluorochrome conjugates. *J. Am. Chem. Soc.* **123**, 12123 (2001).

23. J. Mukhopadhyay, V. Mekler, E. Kortkhonjia, A. Kapanidis, Y. Ebright, R.H. Ebright, Fluorescence resonance energy transfer (FRET) in analysis of transcription-complex structure and function. *Meths. Enzymol.* **371**, 144 (2003).
24. K. Igarashi, A. Ishihama, Bipartite functional map of the *E. coli* RNA polymerase α subunit: Involvement of the C-terminal region in transcription activation by cAMP-CRP. *Cell* **65**, 1015 (1991).
25. C. Vrentas, T. Gaal, W. Ross, R.H. Ebright, R. Gourse, Response of RNA polymerase to ppGpp: requirement for the ω subunit and relief of this requirement by DksA. *Genes Dev.* **19**, 2378 (2005).
26. H. Tang, K. Severinov, A. Goldfarb, D. Fenyo, B. Chait, R. Ebright, Location, structure, and function of the target of a transcription activator protein. *Genes Dev.* **8**, 3058 (1994).
27. K. Severinov, R. Mooney, S. A. Darst, R. Landick, Tethering of the large subunits of *Escherichia coli* RNA polymerase. *J. Biol. Chem.* **272**, 24137 (1997).
28. S. Tuske, Sarafianos, X. Wang, B. Hudson, E. Sineva, J. Mukhopadhyay, J. Birktoft, O. Leroy, S. Ismail, A. Clark, C. Dharia, A. Napoli, O. Laptenko, J. Lee, S. Borukhov, R.H. Ebright, E. Arnold, Inhibition of bacterial RNA polymerase by streptolydigin: stabilization of a straight-bridge-helix active-center conformation. *Cell* **122**, 541 (2005).
29. N. Naryshkin, Y. Kim, Q. Dong, R.H. Ebright, Site-specific protein-DNA photocrosslinking: analysis of bacterial transcription initiation complexes. *Meths. Mol. Biol.* **148**, 337 (2001).
30. H. Takano, M. Kondo, N. Usui, T. Usui, H. Ohzeki, R. Yamazaki, M. Washioka, A. Nakamura, T. Hoshino, W. Hakamata, T. Beppu, K. Ueda, Involvement of CarA/LitR and CRP/FNR family transcriptional regulators in light-induced carotenoid production in *Thermus thermophilus*. *J. Bacteriol.* **193**, 2451 (2011).
31. K. Gaston, A. Bell, A. Kolb, H. Buc, S. Busby, Stringent spacing requirements for transcription activation by CRP. *Cell* **62**, 733 (1990).
32. G. Panaghie, S. Aiyar, K. Bobb, R. Hayward, P. deHaseth, Aromatic amino acids in region 2.3 of *Escherichia coli* σ70 participate collectively in the formation of an RNA polymerase-promoter open complex. *J. Mol. Biol.* **299**, 1217 (2000).
33. R. Hartmann, V. Erdmann, *Thermus thermophilus* 16S rRNA is transcribed from an isolated transcription unit. *J. Bacteriol.* **171**, 2933 (1989).
34. R. Dickson, J. Abelson, P. Johnson, W. Reznikoff, W. Barnes, Nucleotide sequence changes produced by mutations in the *lac* promoter of *Escherichia coli*. *J. Mol. Biol.* **111**, 65 (1977).
35. W. Ross, K. Gosink, J. Salomon, K. Igarashi, C. Zou, A. Ishihama, K. Severinov, R. Gourse, A third recognition element in bacterial promoters: DNA binding by the alpha subunit of RNA polymerase. *Science* **262**, 1407 (1993).
36. J. Mukhopadhyay, K. Das, S. Ismail, D. Koppstein, M. Jang, B. Hudson, S. Sarafianos, S. Tuske, J. Patel, R. Jansen, H. Irschik, E. Arnold, R.H. Ebright, The RNA polymerase "switch region" is a target for inhibitors. *Cell* **135**, 295 (2008).
37. T. Belyaeva, J. Bown, N. Fujita, A. Ishihama, S. Busby, Location of the C-terminal domain of the RNA polymerase alpha subunit in different complexes at the Escherichia coli galactose operon regulatory region. *Nucl. Acids Res.* **24**, 2243 (1996).
38. J. Sambrook, D. Russell, *Molecular Cloning: A Laboratory Manual* (Cold Spring Harbor Laboratory, Cold Spring Harbor, NY, 2001), pp.
39. T. Heyduk, Y. Ma, H. Tang, R.H. Ebright, Fluorescence anisotropy: rapid, quantitative assay for protein-DNA and protein-protein interaction. *Meths. Enzymol.* **274**, 492 (1996).
40. H. Chen, H. Tang, R.H. Ebright, Functional interaction between RNA polymerase α subunit C-terminal domain and σ70 in UP-element- and activator-dependent transcription. *Mol. Cell* **11**, 1621 (2003).
41. W. McClure, Rate-limiting steps in RNA chain initiation. *Proc. Natl. Acad. Sci. USA* **77**, 5634 (1980).
42. G. Gussin, Kinetic analysis of RNA polymerase-promoter interactions. *Meths. Enzymol.* **274**, 45 (1996).

43. Z. Otwinowski, W. Minor, Processing of X-ray diffraction data collected in oscillation mode. *Meths. Enzymol.* **276**, 307 (1997).
44. Collaborative Computational Project Number 4, The CCP4 suite: programs for protein crystallography. *Acta Cryst. D* **50**, 760 (1994).
45. P. Emsley, B. Lohkamp, W. Scott, K. Cowtan, Features and development of Coot. *Acta Cryst. D* **66**, 486 (2010).
46. P. Adams, P. Afonine, G. Bunkóczi, V. Chen, I. Davis, N. Echols, J. Head, L. Hung, G. Kapral, R. Grosse-Kunstleve, A. McCoy, N. Moriarty, R. Oeffner, R. Read, D. Richardson, J. Richardson, T. Terwilliger, P. Zwart, PHENIX: a comprehensive Python-based system for macromolecular structure. *Acta Cryst. D* **66**, 213 (2010).
47. H. Aiba, S. Fujimoto, N. Ozaki, Molecular cloning and nucleotide sequencing of the gene for *E. coli* cAMP receptor protein. *Nucl. Acids Res.* **10**, 1345 (1982).
48. P. Cossart, B. Gicquel-Sanzey, Cloning and sequence of the *crp* gene of *Escherichia coli*. *Nucl. Acids Res.* **10**, 1363 (1982).
49. E. Campbell, O. Muzzin, M. Chlenov, J. Sun, C. Olson, O. Weinman, M. Trester-Zedlitz, S. Darst., Structure of the bacterial RNA polymerase promoter specificity σ subunit. *Mol. Cell* **9**, 527 (2002).
50. D. Vassylyev, M. Vassylyeva, A. Perederina, T. Tahirov, I. Artsimovitch, Structural basis for transcription elongation by bacterial RNA polymerase. *Nature* **448**, 157 (2007).
51. G. Parkinson, C. Wilson, A. Gunasekera, Y. Ebright, R.H. Ebright, H. Berman, Structure of the CAP-DNA complex at 2.5 Å resolution: a complete picture of the protein-DNA interface. *J. Mol. Biol.* **260**, 395 (1996).
52. K. Murakami, The x-ray crystal structure of *Escherichia coli* RNA polymerase sigma70 holoenzyme. *J. Biol. Chem.* **288**, 9126 (Feb 6, 2013).
53. B. Bae, E. Davis, D. Brown, E. Campbell, S. Wigneshweraraj, S. Darst, Phage T7 Gp2 inhibition of *Escherichia coli* RNA polymerase involves misappropriation of σ70 domain 1.1. *Proc. Natl. Acad. Sci. USA* **110**, 19772 (Dec 3, 2013).
54. D. Degen, Y. Feng, Y. Zhang, K. Ebright, Y. Ebright, M. Gigliotti, H. Vahedian-Movahed, S. Mandal, M. Talaue, N. Connell, E. Arnold, W. Fenical, R.H. Ebright, Transcription inhibition by the depsipeptide antibiotic salinamide A. *eLife* **3**, e02451 (2014).
55. N. Naryshkin, A. Revyakin, Y. Kim, V. Mekler, R. Ebright, Structural organization of the RNA polymerase-promoter open complex. *Cell* **101**, 601 (2000).